telecom

MDPI

Article

Physics-Inspired Convolutional Neural Network for Scalable Modeling of Radio Wave Propagation

Oluwole John Famoriji [1,2,*], Michael O. Omojoyegbe [2,3] and Ebenezer Esenogho [2]

[1] Department of Electrical and Electronics Engineering, Faculty of Engineering and Technology, Federal University of Technology and Environmental Sciences, P. M. B. 001, Iyin-Ekiti 360101, Nigeria
[2] Centre for Artificial Intelligence and Multidisplinary Innovations Studies, University of South Africa, Peller Street, Pretoria 0002, South Africa
[3] Department of Electrical and Information Engineering, Faculty of Engineering and Technology, Achievers University, KM 1, Idasen/Uteh Road, P. M. B. 1030, Owo 341104, Nigeria
* Correspondence: oluwole.famoriji@futes.edu.ng

Abstract

Reliable estimation of radio wave propagation across irregular terrain is essential for the effective planning and optimization of contemporary wireless communication systems, such as cellular networks, broadcasting infrastructure, and radar systems. The intricate interaction between electromagnetic waves and environmental features—including mountains, depressions, and artificial structures—requires sophisticated modeling approaches capable of accounting for diffraction, reflection, scattering, and shadowing effects caused by terrain variations. The use of the split-step parabolic equation (SSPE) method for modeling radio wave propagation over irregular terrain has become increasingly popular. However, high computational cost limits its practical deployment. This has led to growing interest in machine learning (ML) as a more efficient alternative. A major challenge of ML in electromagnetic applications lies in accurately predicting results for scenarios not represented in the training data—a limitation not yet fully addressed by existing ML-based propagation models. To overcome this challenge, a high-fidelity, scalable physics-inspired modeling framework is presented. The proposed method effectively adapts to various terrain profiles and antenna setups, demonstrating strong extrapolation performance beyond the training set. Furthermore, another key innovation is the integration of prior knowledge from deterministic physics-based models into the neural network architecture. Additionally, tailoring the network structure to reflect the physical characteristics of terrain-based wave propagation significantly enhances both prediction accuracy and scalability.

Keywords: convolutional neural network; physics-inspired; radio wave propagation; irregular terrain; parabolic wave equation; scalable

Check for updates

Academic Editor: Sotirios K. Goudos

Received: 17 March 2026
Revised: 22 June 2026
Accepted: 24 June 2026
Published: 3 August 2026

Copyright: © 2026 by the authors. Licensee MDPI, Basel, Switzerland. This article is an open access article distributed under the terms and conditions of the Creative Commons Attribution (CC BY) license.

1. Introduction

Accurate modeling of radio wave propagation over irregular terrain is fundamental to the planning, design, and optimization of modern wireless communication systems. Traditional methods, such as ray tracing, parabolic equation methods, and empirical models like the Longley–Rice model, have served as the backbone for understanding signal behavior across complex terrains [1,2]. However, these methods often require extensive computational resources, are sensitive to terrain resolution, and struggle to generalize across diverse environmental conditions. With the increasing demands of fifth- and sixth-generation (5G/6G) networks, Internet of Things (IoT) deployments, and rural connectivity

initiatives, there is a growing need for efficient, scalable, and generalizable models that can accurately predict signal behavior in real-world settings. In recent years, deep learning techniques, particularly convolutional neural networks (CNNs), have shown great promise in approximating complex physical phenomena by learning directly from data. However, purely data-driven models often lack physical interpretability and may fail when applied outside their training domains. To address this, we propose a physics-inspired CNN framework that integrates prior knowledge from deterministic propagation models into the learning architecture. By embedding physical parameters and spatial context into the model, we aim to achieve both high accuracy and generalizability in radio wave propagation prediction across diverse and irregular terrain profiles.

Conventional radio propagation models, including the Okumura–Hata, International Telecommunication Union-Radiocommunication (ITU-R), and Longley–Rice models, rely on simplified empirical relationships or deterministic formulations to estimate path loss over various environments [1]. While these models are computationally efficient, their accuracy diminishes in highly variable terrains and complex propagation scenarios. Ray tracing and parabolic equation methods offer improved fidelity by simulating the physical behavior of electromagnetic waves, but they are computationally intensive and often infeasible for large-scale or real-time applications. The two-way split-step parabolic equation (SSPE) method has become a reliable and computationally efficient tool for modeling propagation in complex environments [3–9]. However, its practicality is hindered by the need to rerun simulations whenever there are minor changes in terrain features or antenna configurations. Additionally, the method is not well-suited for real-time applications due to its computational demands. To overcome these challenges, recent studies have turned to machine learning (ML) techniques. In [10], a propagation model based on CNNs was proposed to predict path loss at specific heights. However, its applicability was confined to a limited range of terrain profiles and did not account for antenna parameters, thereby restricting its ability to generalize across different configurations. To overcome these limitations, recent studies have explored the application of machine learning (ML) to propagation modeling. Works by Famoriji and Shongwe (2025) [11] and Ma et al. (2020) [12] have applied random forests and support vector machines for predicting signal strength, while other studies have used deep neural networks for site-specific path loss prediction, such as Mylonakis et al. [8] and Zhang et al. [9]. Although these models improve prediction accuracy and reduce runtime, they typically require extensive retraining for different terrains and do not integrate prior physical knowledge, limiting their scalability.

Despite these advantages, conventional PINNs face several challenges, including difficulties in training deep networks, spectral bias toward low-frequency solutions, convergence issues in stiff or multi-scale systems, and reduced accuracy when dealing with complex geometries or highly oscillatory phenomena [4]. To address these limitations, numerous PINN variants and extensions have been proposed, such as adaptive loss-weighting strategies, domain decomposition approaches, multi-network architectures, curriculum learning techniques, Fourier-feature embeddings, and hybrid physics–machine learning frameworks. These developments collectively represent an active research landscape aimed at improving the robustness, scalability, and accuracy of physics-informed learning.

Within this broader context, wave and propagation problems constitute a particularly demanding class of applications for PINNs. Propagation phenomena are typically governed by hyperbolic or wave-type PDEs and often exhibit high-frequency oscillations, long-range dependencies, sharp gradients, and multi-scale dynamics. Examples include electromagnetic wave propagation, acoustic transmission, seismic wave modeling, optical signal propagation, and other transport-related physical processes [5]. The oscillatory nature of these solutions can exacerbate the spectral bias of standard neural networks, making

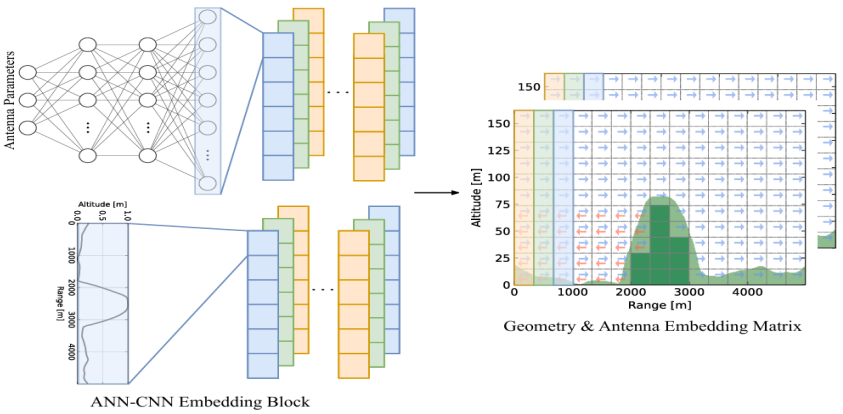
accurate representation and convergence more challenging than in diffusion-dominated or steady-state problems.

Recent studies have therefore focused on adapting PINN methodologies specifically for propagation-related applications. These efforts include the incorporation of enriched feature representations, frequency-aware network architectures, adaptive sampling techniques, and physics-guided regularization strategies to better capture wave characteristics and improve solution fidelity [7]. Such approaches have demonstrated improved performance in modeling complex propagation dynamics while maintaining the fundamental advantages of physics-informed learning.

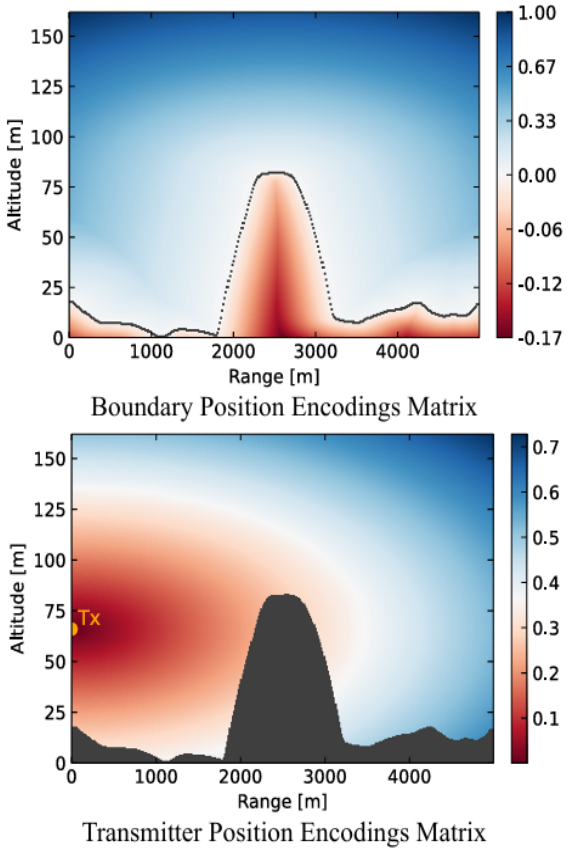
More recently, physics-informed neural networks (PINNs) and hybrid models have emerged as a promising direction, embedding physical laws into data-driven models. In the context of wireless propagation, this approach remains underexplored. Existing models such as PhysNet and GeoNet [4–7] have shown success in fields like fluid dynamics and seismic modeling by blending data with domain knowledge. Inspired by these advancements, our approach leverages a CNN architecture augmented with terrain-aware features and deterministic model outputs, allowing the network to learn spatial dependencies while respecting underlying physical principles [12–15]. Despite progress, few studies have addressed the challenge of scalable modeling over diverse terrain profiles while maintaining physical consistency. To close this gap, we introduce a scalable terrain propagation framework capable of delivering high-accuracy predictions across diverse terrain configurations and antenna parameters. Notably, our model demonstrates the ability to extrapolate up to 1.67 times beyond its original training range, as confirmed through test scenarios involving antenna parameters—such as height, tilt angle, and beamwidth—that exceeded the bounds of the training data.

In ref. [16], a CNN-based propagation model was created to predict path loss at specific heights. However, this model was restricted to particular terrain profiles and did not account for antenna parameters or generalize across them. To address this limitation, we introduce a generalizable terrain propagation framework that delivers high accuracy across diverse terrain profiles and antenna parameters. Importantly, our model can extrapolate its performance up to 1.67 times beyond the training range, as demonstrated through tests involving antenna parameters like height, tilt angle, and beamwidth that exceeded the training limits. The workflow of our method is shown in Figure 1a–c.

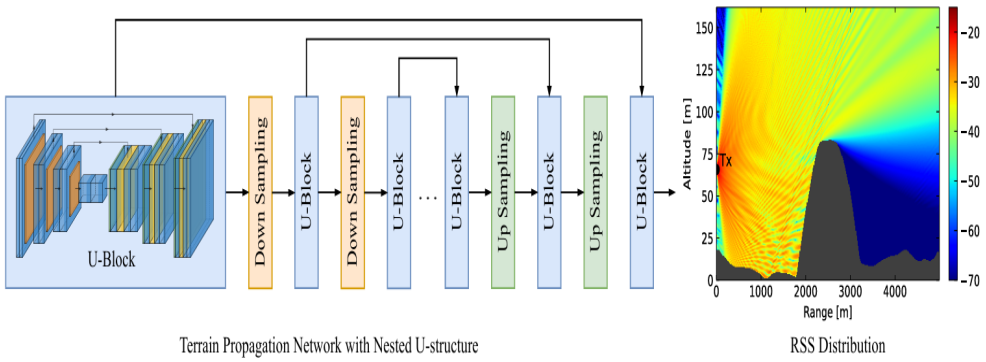
To build this generalizable framework, three key challenges have been addressed in this paper. The most significant challenge—and the main contribution—lies in designing physics-guided features that the model can effectively interpret. Prior studies on generalizable surrogate models mostly relied on features used in traditional empirical models, directly feeding these into neural networks [17–19]. Such features often occupy high-dimensional spaces but contain sparse meaningful information, which weakens the influence of important details and makes it difficult for the model to learn effectively. Furthermore, this input format limits the network's ability to capture complex relationships between features, restricting its generalization capabilities. To bridge this gap, we propose a physics-guided embedding method. By explicitly integrating prior knowledge from the SSPE method into the embedding layer design, we convert terrain profiles and antenna parameters into dense matrices that the network can interpret. Incorporating this prior knowledge simplifies training and guides the learning process. The features generated by our embedding layer greatly improve the model's generalizability and accuracy. Moreover, to boost prediction precision over large spatial ranges, we include positional encodings as additional features, which capture the distances from each receiver to both the transmitter and the terrain surface, thus providing valuable spatial context.



(**a**)



(**b**)



(**c**)

Figure 1. Diagram illustrating the proposed scheme. (**a**) Physics-informed parameter embedding. (**b**) Position encoding. (**c**) Terrain propagation network-based nonlinear mapping.

The second challenge concerns the choice of modeling approach. The existing model [16] lacks the ability to generalize antenna parameters because its sequential, path loss–based method cannot adequately capture the intricate interactions between antenna characteristics and terrain geometry. We overcome this limitation by modeling propagation across two spatial dimensions. The third challenge involves creating a network architecture specifically optimized for terrain propagation scenarios. Since irregular terrain features cause multipath effects that produce complex waveforms with sharp spatial gradients, and because generalizing over antenna parameters requires processing abstract semantic information, the network must combine sufficient depth with the preservation of high-resolution feature maps. To our knowledge, current models [20–24] do not fulfill both these criteria. To address this, we propose a nested U-structure, which we call the terrain propagation network (TPN).

The paper proposes a convolutional neural network architecture that incorporates prior knowledge from deterministic split-step parabolic equation (SSPE)-based propagation models to improve scalability, prediction accuracy, and generalization to unseen terrain and antenna configurations. The study particularly addresses the challenge of extrapolation beyond the training dataset, demonstrating that the proposed framework can effectively model complex electromagnetic propagation phenomena while significantly reducing computational cost compared to conventional SSPE approaches. We propose the use of CNNs for two-dimensional (2D) prediction of radio wave propagation over irregular terrain. The CNN training process is based on data generated using computationally intensive two-way SSPE simulations. The presented results demonstrate that the proposed approach can provide sufficiently accurate approximations of conventional SSPE calculations while, at the same time, significantly reducing the computation time required for propagation prediction. In summary, the proposed method effectively adapts to various terrain profiles and antenna setups, demonstrating strong extrapolation performance beyond the training set. Furthermore, another key innovation is the integration of prior knowledge from deterministic physics-based models into the neural network architecture. Additionally, tailoring the network structure to reflect the physical characteristics of terrain-based wave propagation significantly enhances both prediction accuracy and scalability.

The structure of this paper is organized as follows: Section 2 introduces the proposed scalable physics-guided terrain propagation model, including the data generation methodology and implementation specifics. Section 3 details the ablation studies performed on the network architecture and feature components, providing a quantitative evaluation of each proposed method. This section also showcases the model's interpolation and extrapolation capabilities with respect to both terrain profiles and antenna parameters. In Section 4, we validate the model using measured data from two real-world scenarios. Finally, Section 5 presents the conclusions, limitations, and future directions of this study.

2. Terrain Propagation Model Enhanced by Machine Learning

2.1. Bidirectional Split-Step Parabolic Equation Method

In our proposed model, the training dataset is generated using the two-way SSPE method [25], which is based on the Helmholtz wave equation. This approach decomposes the wave into two parts that propagate in the forward and backward directions, effectively handling obstacles, as shown by the blue and red arrows in Figure 1a–c. The field distribution at each cross-section along the wave's path is computed from the preceding cross-section using an update formula.

$$u(x, y, z + \Delta z) = F^{-1}\{C(k_x)C(k_y)F\{u(x, y, z)\}\} \quad (1)$$

Here, F and F^{-1} represent the Fourier transform and its inverse; k_x and k_y denote the spectral variables; and u corresponds to the reduced plane wave solution.

$$C(k_\varsigma) = \exp\left(\frac{-jk_\varsigma^2 \Delta z}{2k_0}\right) \tag{2}$$

where ς represents either x or y, and k_0 is the free-space wavenumber. The backward-propagating waves are updated according to

$$u(x, y, z - \Delta z) = F^{-1}\{C(k_x)C(k_y)F\{u(x, y, z)\}\}. \tag{3}$$

Further information about the two-way SSPE method is available in [12,13].

2.2. Physics-Informed Parameter Integration

The approach used to integrate terrain profiles and antenna parameters into the network plays a crucial role. Since these inputs are inherently low-dimensional, they limit the model's capacity to generalize effectively. To overcome this limitation, an embedding layer is introduced to convert these inputs into rich, high-dimensional feature representations. This layer learns a feature space that captures the complex, nonlinear relationships between the antenna parameters and the terrain profile. By refining these representations during training, the embedding layer captures transferable patterns that improve the model's predictive accuracy on previously unseen data.

Next, we developed a tailored embedding method. Due to the large gap between the input and output dimensions, the standard fully connected network-based embedding layer—illustrated in Figure 2b—introduces excessive complexity and proves ineffective. To resolve this, we redesigned the embedding layer by drawing inspiration from the SSPE (Split-Step Parabolic Equation) method. In SSPE simulations, wave propagation is modeled through a series of iterative vector updates, where each update reflects the local environmental conditions at a given spatial point. This iterative nature captures the gradual evolution of the wavefield. Motivated by this, we represent antenna parameters or terrain profiles as individual feature vectors using a fully connected layer. These vectors are then expanded along the channel dimension using one-dimensional (1D) convolutions, gradually increasing the number of channels to match the number of iterations in the SSPE process. As shown in Figure 2a, each resulting channel encodes the local environmental context relevant for one SSPE iteration. Finally, we convert the channel dimension into the range dimension of the feature map, aligning the representation with the spatial progression of wave propagation.

This redesigned embedding strategy improves parameter efficiency by leveraging physical insights from SSPE. The progressive convolutional expansion utilizes spatial dependencies in terrain data and mirrors the continuous nature of wave propagation. The effectiveness of this physics-guided embedding method compared to traditional approaches is further detailed in Section 3.1.

2.3. Encoding of Receiver Location

We found that using only feature embeddings as input causes predictions at positions distant from the transmitter and terrain boundaries to become overly smoothed. This suggests the model struggles to accurately learn the spatial relationships between the transmitter, receivers, and surrounding terrain features. To address this issue, we incorporated boundary-based and transmitter-based position encodings into the model to supply it with crucial spatial context. The effectiveness of this position encoding strategy is analyzed in Section 3.1.

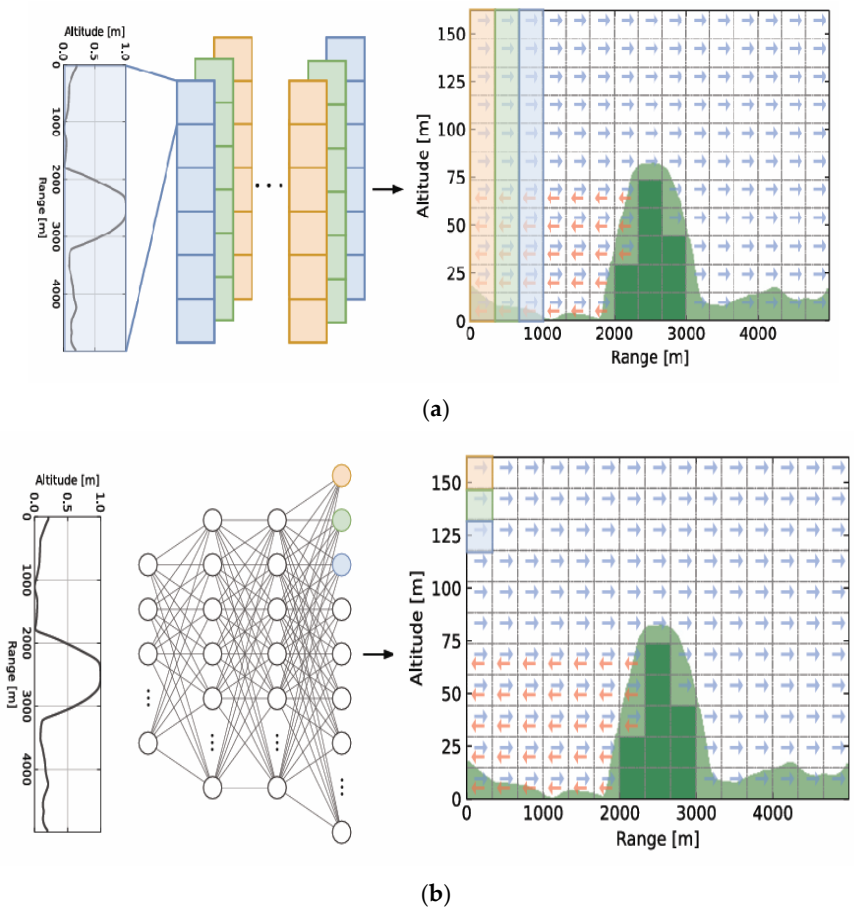


Figure 2. Illustration of the physics-guided embedding framework for terrain-aware wave propagation modeling. (**a**) Designed physics-informed embedding module. (**b**) Conventional embedding layer without prior physical information.

To represent each point's spatial relation to the terrain surface, this encoding treats the boundary as zero, assigns positive values to points above the surface (in the air), and negative values to those below it. The absolute value reflects the distance from the boundary. Specifically, we begin by generating the terrain surface set for a given profile. Based on the terrain's discrete representation on a Cartesian grid, this surface set consists of coordinate points (i, j) that define the terrain boundary within a domain $\Omega \subset R^2$.

$$S = \left\{ (i,j) \in R^2 : f(i,j) = 0 \right\} \tag{4}$$

Here, f represents the surface function, where $f\ (i, j) = 0$ if and only if the point (i, j) lies exactly on the terrain surface. If $f(i, j) < 0$, the point is located beneath the surface, and if $f(i, j) > 0$, the point lies above the surface. The boundary distance function $D(i, j)$, corresponding to the surface function $f(i, j)$, is defined as follows:

$$D(i,j) = \min_{(i'j') \in Z} \left| (i,j) - (i',j') \right| sign(f(i,j)) \tag{5}$$

The function $D(i, j)$ serves as a signed distance function, quantifying how far a point (i, j) is from the nearest boundary of set S, with the sign indicating whether the point lies above or below the surface.

For transmitter position encoding, each point captures its distance from the transmitter's location. Any points situated on or below the surface are assigned a value of -1.

Specifically, if the transmitter is located at coordinates (t_{xi}, t_{xj}), the transmitter distance function $D'(i, j)$ is defined as follows:

$$D'(i,j) = \begin{cases} \sqrt{(i - \mathbf{t}X_i)^2 + (j - \mathbf{t}X_j)^2} & if\ f(i,j) > 0 \\ -1 & otherwise \end{cases} \quad (6)$$

2.4. Terrain-Based Propagation Network Architecture

The Terrain Propagation Network (TPN) is specifically designed to satisfy three core requirements: adequate network depth, preservation of high-resolution feature maps, and the ability to learn across multiple scales. Adequate depth ensures the network can perform the complex nonlinear transformations needed to generalize antenna parameters effectively. High-resolution feature maps are crucial for modeling multipath effects caused by irregular terrain. These effects produce intricate waveforms with sharp spatial gradients due to wave superposition and interference, which would be lost if the feature maps were overly smoothed. Multi-scale learning is essential for capturing terrain effects at various levels: macro-scale (e.g., mountain ranges influencing long-distance propagation), meso-scale (e.g., hills causing scattering), and micro-scale (e.g., diffraction from fine surface details).

Achieving both depth and high resolution simultaneously poses a challenge because deeper networks often come with increased computational and memory demands. Some existing models increase depth at the cost of spatial resolution [26], while others, like U-Net variants, maintain resolution but lack the depth needed to fully model complex propagation patterns [27]. To address this trade-off, the TPN employs a nested U-shaped architecture [28–30], as illustrated in Figure 3c. At the top level, it adopts a standard U-Net structure to retain high-resolution features. Within each stage, a basic block integrates another U-shaped structure (see Figure 3a,b), allowing for complex nonlinear representation while keeping computational costs manageable via pooling operations. This hierarchical design not only supports deep modeling but also enhances multi-scale feature extraction within each block. In deeper layers like E5, E6, and D5, where input feature maps already have low resolution, atrous (dilated) convolutions are used in place of further down-sampling to avoid losing crucial spatial information.

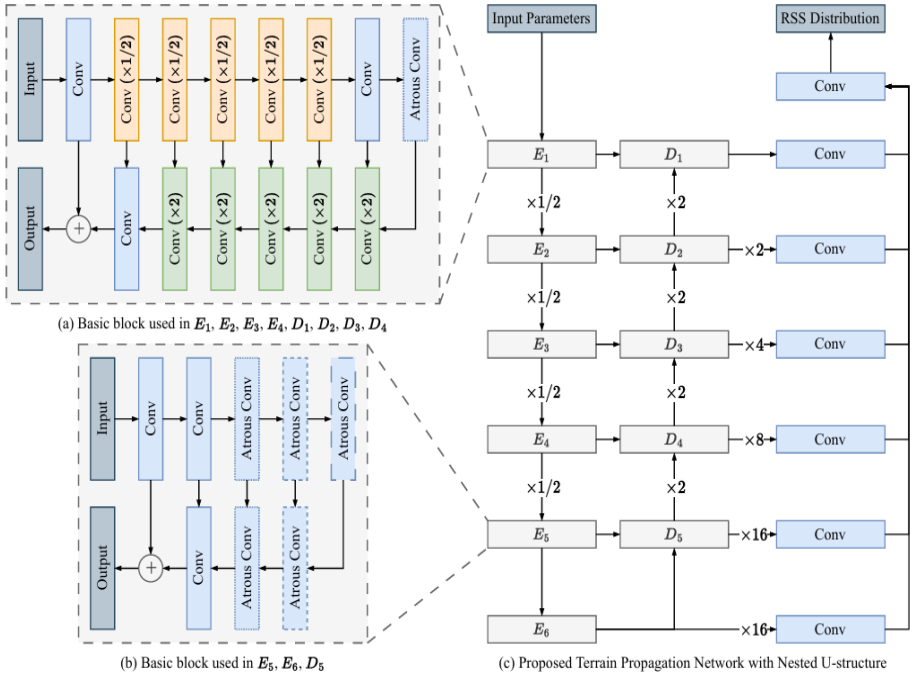


Figure 3. Proposed terrain propagation network featuring a nested U-shaped architecture.

3. Numerical Experiment and Results

This section compares the traditional SSPE method with the proposed physics-guided CNN model across different scenarios to validate the effectiveness of our approach. During training, a terrain length of 5000 m is used, with a unit strength Gaussian source positioned at the initial cross-section. The operating frequency is set at 1 GHz, and the detailed input parameters for the SSPE method are outlined in Table 1. For spatial discretization in the SSPE method, step sizes of $\Delta x = 25\lambda$ and $\Delta y = 0.5\lambda$ are selected based on the recommendations in [2].

Table 1. Configuration of input parameters for the SSPE simulation.

Parameter	Minimum Value	Maximum Value	Increment
Terrain Profile [°]	−0.35	0.35	0.065
Beamwidth [°]	15	30	1
Elevation Angle [°]	0	15	1
Antenna Height [m]	5	20	1

In addition to the parameters listed in Table 1, randomized terrain profiles are generated using Perlin noise [31]. This method is advantageous due to its ability to produce smooth and continuous gradients, which is crucial for modeling realistic terrain features where elevation transitions are gradual and natural rather than sudden or abrupt. Specifically, each layer of Perlin noise is generated from a discrete sequence of random gradient values g_u (where $u \in Z$), uniformly distributed over the interval $[-1, 1]$ [32]. The resulting noise function $N(x)$ is then calculated through piecewise interpolation, using a local function F at points x ∈ R, as defined below

$$N(x) = F(x, g_u, g_{u+1}), \quad where\ u = \lfloor x \rfloor \tag{7}$$

By summing multiple layers of scaled Perlin noise with K distinct frequencies and amplitudes, we can systematically analyze how terrain features at various scales influence electromagnetic wave propagation. Consequently, the final form of the Perlin noise utilized in this study is defined as follows [33]:

$$PN(x) = \sum_{i=0}^{K-1} a_i \cdot N(f_i \cdot x) \tag{8}$$

where each frequency f_i is calculated using the expression: $f_i = f_{min}\left(\frac{i-1}{K-1}\right) + f_{min}$ and each amplitude a_i by $a_i = a_{max}\left(1 - \frac{i-1}{K-1}\right)\exp(-b(i-1))$. This setup enables a detailed examination of how terrain features at different scales influence electromagnetic wave propagation.

We further enhanced the diversity of terrain profiles by adding a linear gradient characterized by a slope angle θ. The resulting terrain elevation $y(x)$ is obtained by superimposing this linear trend onto the Perlin noise function.

$$y(x) = \alpha \cdot PN(x) + \beta \cdot \tan(\theta) \cdot x \tag{9}$$

To maintain consistency between the generated profiles and realistic irregular terrains depicted in [34], we adjusted the parameters as follows: f_{min} = 0.001, K = 50, a_{max} = 10, b = 0.35, α = 3, and β = 1. Importantly, this random generation process was applied individually to each terrain profile, resulting in a total of 45,056 distinct profiles used in this study.

For the network's hyperparameters, the proposed embedding block begins with two fully connected layers containing 64 and 128 neurons, respectively, followed by a third layer with neurons corresponding to the number of altitude grid points. This is followed by two 1D convolutional layers with 64 and 128 channels, and a final layer with a number of channels matching the iterations in the SSPE method. All convolutional layers use a kernel size of 3 and a stride of 1. Max pooling is applied with a kernel size and stride of 2.

The training utilizes deep supervision with mean squared error (MSE) loss at each decoder level. An Adam (adaptive moment estimation) optimizer is employed with a dynamic learning rate strategy, starting at 1×10^{-3}. If the training loss does not improve by at least 1×10^{-4} over three consecutive epochs, the learning rate is reduced by a factor of 0.1. An early stopping criterion is also implemented—training halts if the training loss decreases by less than 1×10^{-5} over ten consecutive epochs.

The model was trained on a workstation with an AMD Ryzen 9 7950X CPU (central processing unit) (AMD, Santa Clara, CA, USA) and an NVIDIA GeForce RTX 3090 GPU (graphic processing unit) (NVIDIA, Santa Clara, CA, USA), using a batch size of 4. The full training process took approximately 100 h to complete.

3.1. Evaluation of Proposed Features via Ablation Analysis

In this section, we validate the effectiveness of our newly proposed physics-guided parameter embedding method and position encoding through ablation studies. Keeping the model architecture and implementation fixed, we trained six models with different feature combinations and performed a comparative analysis, as shown in Table 2. For this analysis, we created a dataset with antenna parameters defined in Table 1. Terrain profiles were generated by randomly selecting trends from Table 1 and adding Perlin noise. The dataset was split into 80% for training and 20% for testing, ensuring that both transmitter configurations and terrain profiles in the test set were not seen by the model. All examples discussed here come from the test set.

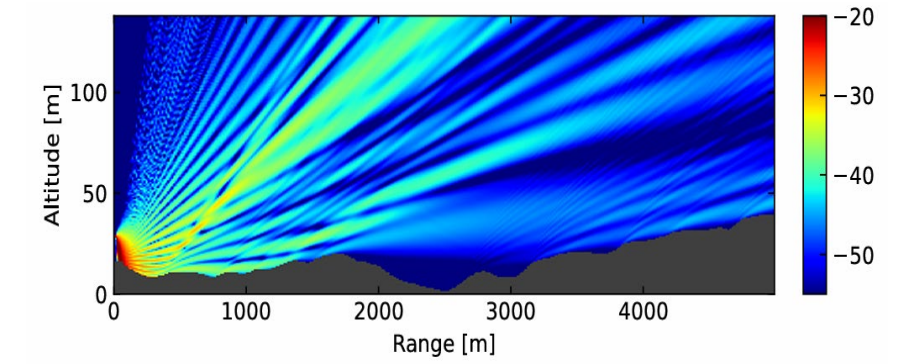
Table 2. Performance evaluation of the developed Feature.

Transmitter Position Encoding	Boundary Position Encoding	Physics-Inspired Addition	Parameters	Validation Loss
Yes	Yes	Yes	44644302	0.00047
No	Yes	Yes	44643726	0.00070
Yes	No	Yes	44643726	0.00053
No	No	Yes	44643150	0.00096
No	No	No	149744013	0.00145

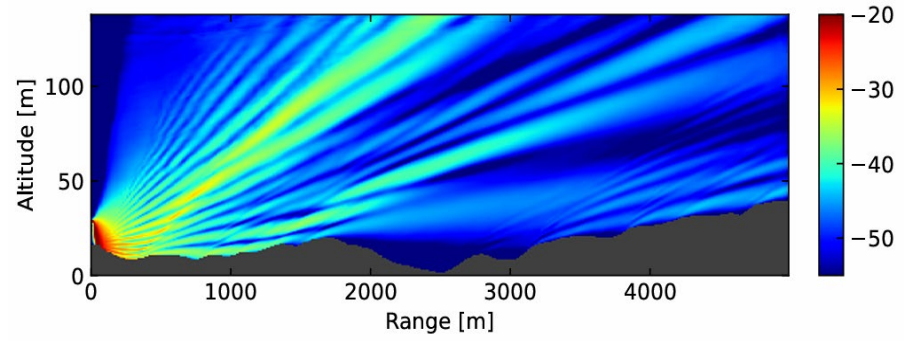
First, we compared the model using a standard embedding, similar to that in [16], with the model incorporating our proposed embedding, as highlighted in the last two rows of Table 2. The validation loss, measured by mean absolute error (MAE), shows that by incorporating prior physical knowledge, our method reduces the model's parameter count by 70% while improving accuracy by 34%. This conclusion is further supported by the results shown in Figures 4a,e,f and 5, demonstrating the high efficiency of our newly proposed physics-guided embedding technique.

Next, we evaluated the model's performance with boundary position encoding and transmitter position encoding against versions without these encodings, as detailed in the first four rows of Table 2. The results show that adding transmitter position encoding alone improves accuracy by 45%, while boundary position encoding alone boosts it by 27%. When both position encodings are applied together, the model's accuracy increases by 52%. These findings are also supported by the data shown in Figures 4a–e and 5.

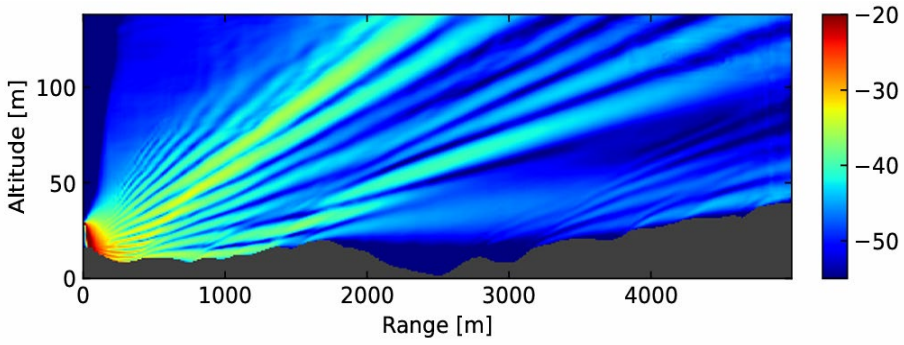
Moreover, comparing Figure 4b,e reveals that adding position encoding greatly enhances the detail and accuracy of predictions, especially for locations far from the transmitter and boundary. This confirms that the position encoding functions as intended and plays a key role in boosting the model's performance. Regarding computation time, the proposed model completes its process in just 0.053 s, whereas the traditional SSPE method takes 782 s, highlighting a substantial speed advantage of our approach.



(**a**)

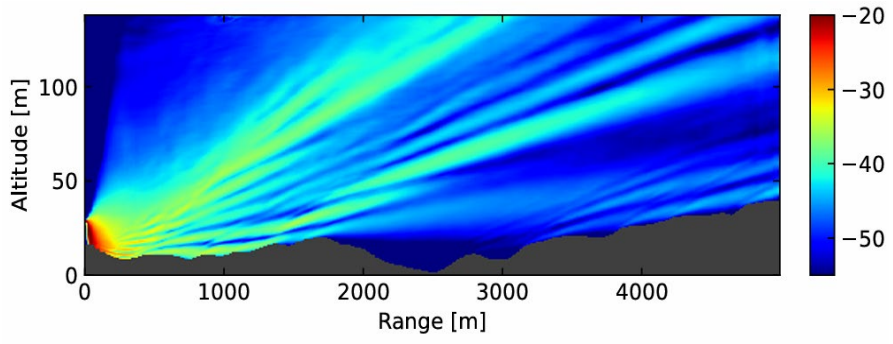


(**b**)

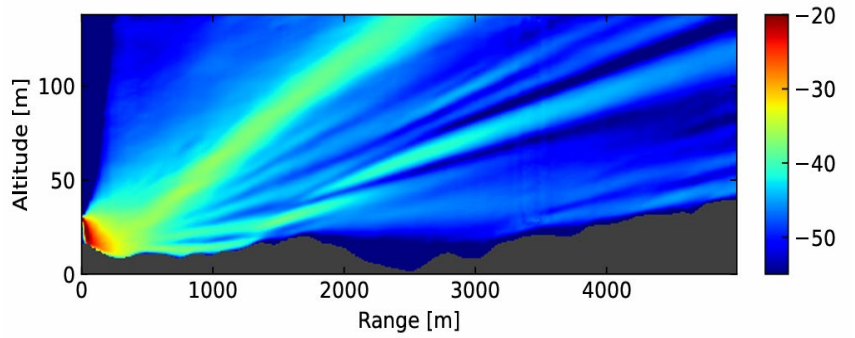


(**c**)

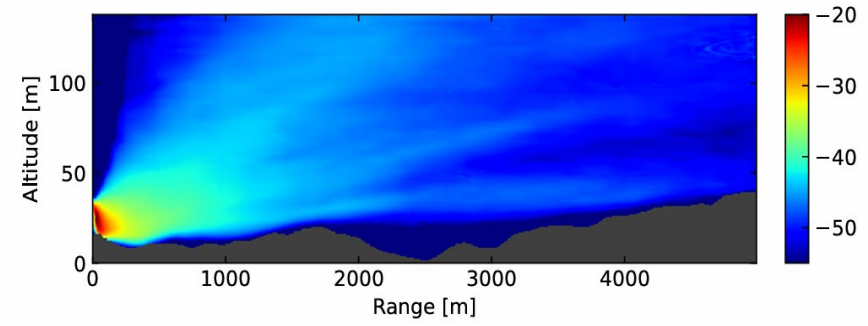
Figure 4. *Cont.*



(**d**)



(**e**)



(**f**)

Figure 4. Field map predictions using various feature sets: (**a**) SSPE, (**b**) all features included, (**c**) all features except the transmitter distance map, (**d**) all features except the boundary distance map, (**e**) terrain profile and antenna parameters embedded using the proposed methods, and (**f**) terrain profile and antenna parameters embedded using conventional methods, as in [16]. The antenna is positioned at a height of 15 m, with a 3 dB beamwidth of 15°, and a tilt angle of 15°.

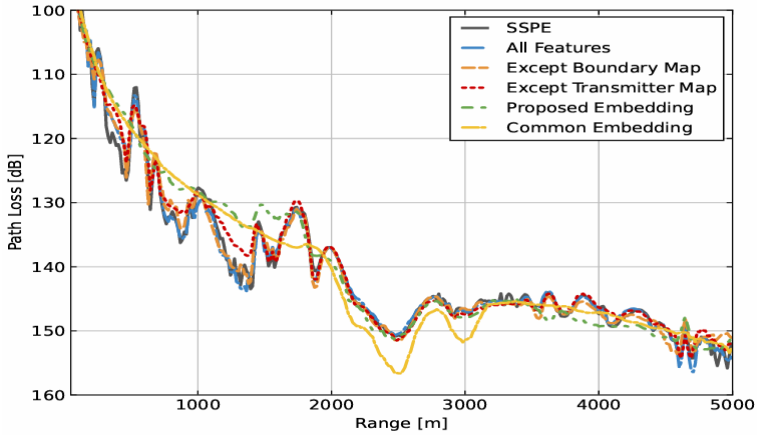
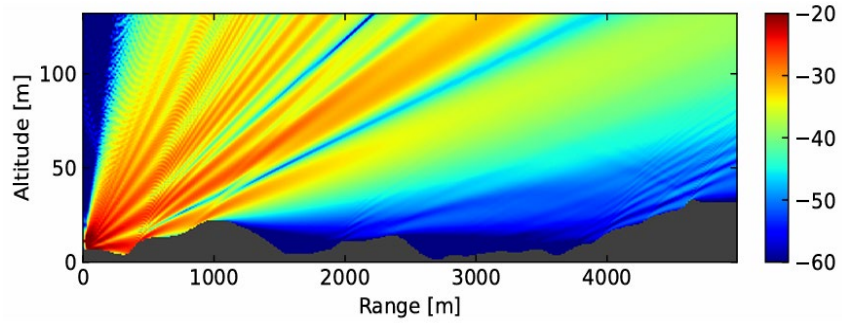


Figure 5. Path loss predictions using various feature sets. The antenna is positioned at a height of 15 m, with a 3 dB beamwidth of 15° and a tilt angle of 15°.

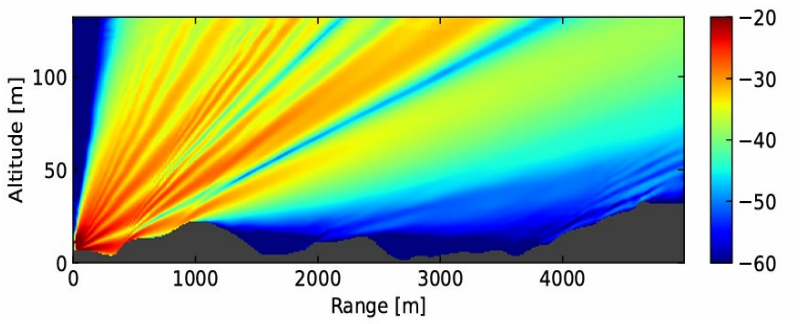
3.2. Comparative Analysis of Convolutional Neural Network Designs

In this section, we validate the performance of our newly developed network architecture. As previously discussed, earlier models can generally be grouped into two main types. The first type prioritizes deeper network structures at the expense of high-resolution feature maps. To represent this group, we selected the influential model introduced by Chen et al. [26], which is widely used across various domains. The second type includes models from the U-Net family, which aim to retain high-resolution feature information. For this category, we chose the model by Huang et al. [27], also known for its broad applicability. Additionally, we included the model proposed by [16]—which uses the original U-shaped U-Net architecture and has been applied to terrain wave propagation—as our baseline. The datasets used for training and testing align with those defined in Section 3.1, and the results shown in this section are taken from the test set.

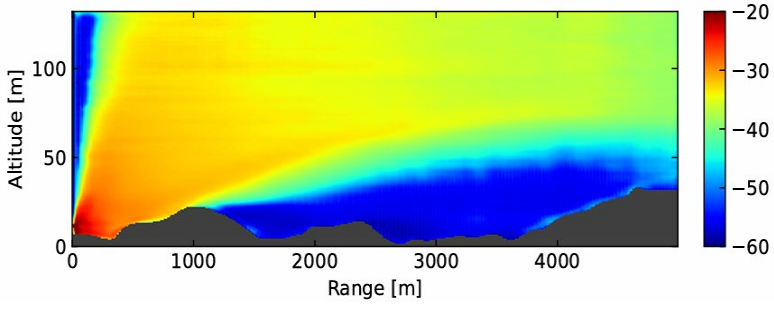
Table 3 shows the quantitative outcomes of the ablation study, using Mean Absolute Error (MAE) to assess the validation loss. Compared to the models proposed by Chen et al. and Brennan et al., our model achieves reductions in parameter count by 21%, 29%, and 85%, respectively, while improving accuracy by 64%, 71%, and 85%. Similar insights are supported by the results in Figures 6 and 7. These findings highlight the substantial advantages of our model, specifically designed for terrain propagation, and underscore its meaningful contribution to the field.



(**a**)

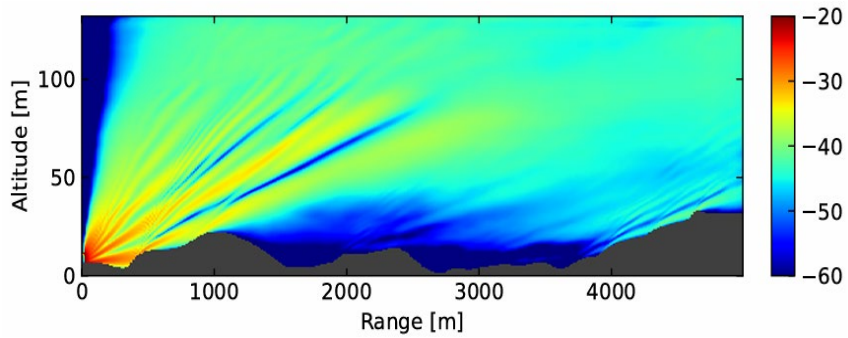


(**b**)

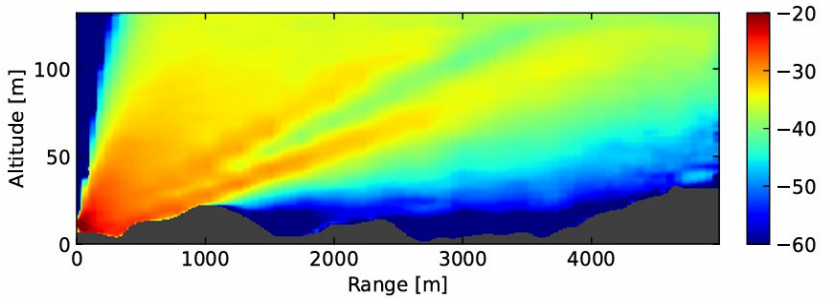


(**c**)

Figure 6. *Cont.*



(**d**)



(**e**)

Figure 6. Field map predictions using different methods: (**a**) SSPE, (**b**) Proposed model, (**c**) U-Net-based approach similar to the model in [26], (**d**) U-Net-based milestone model commonly used in Pix2Pix tasks [27], and (**e**) Depth-wise separable convolution-based milestone model also common in Pix2Pix tasks [26]. The antenna is positioned at a height of 5 m, with a 3 dB beamwidth of 15°, and a tilt angle of 0°.

Table 3. Performance evaluation of the developed network.

Network	Parameter	Validation Loss
Ref. [20]	62481668	0.00161
Ref. [19]	56522722	0.00129
Ref. [9]	288345716	0.00300
This work	44644302	0.00047

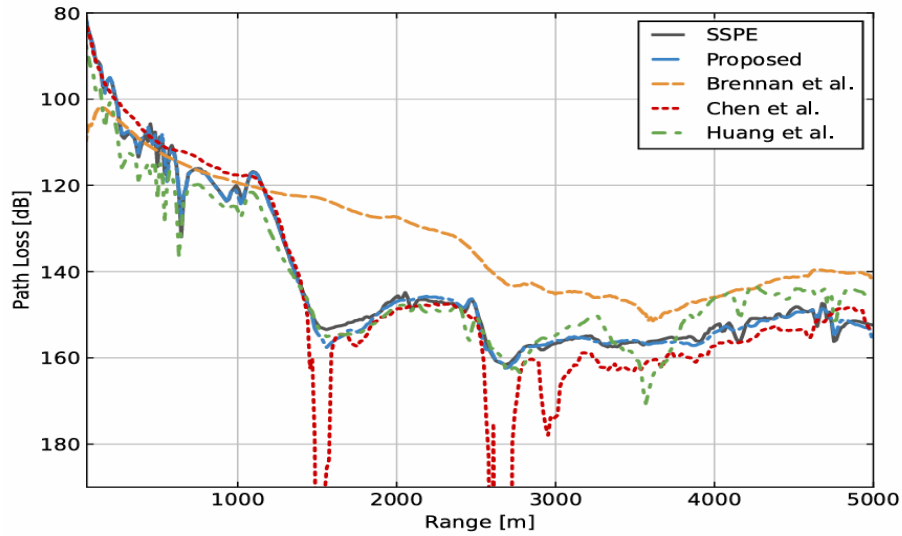
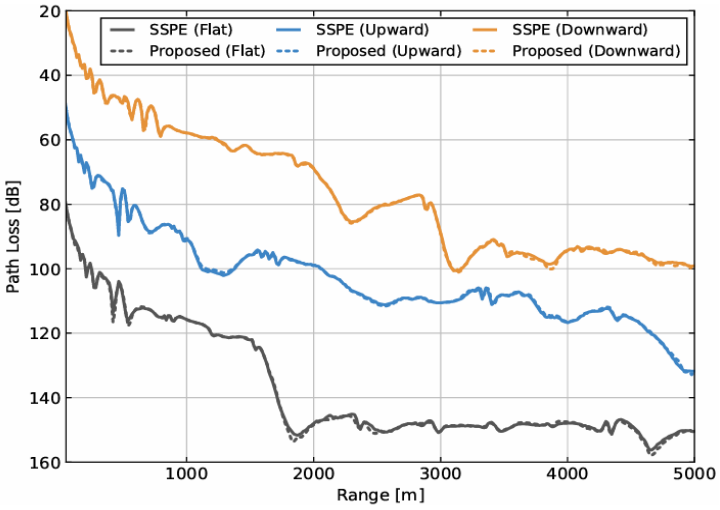


Figure 7. Path loss predictions using various methods. The antenna is positioned at a height of 5 m, with a 3 dB beamwidth of 15°, and a tilt angle of 0° [16,26,27].

3.3. Insights into Generalization Behavior

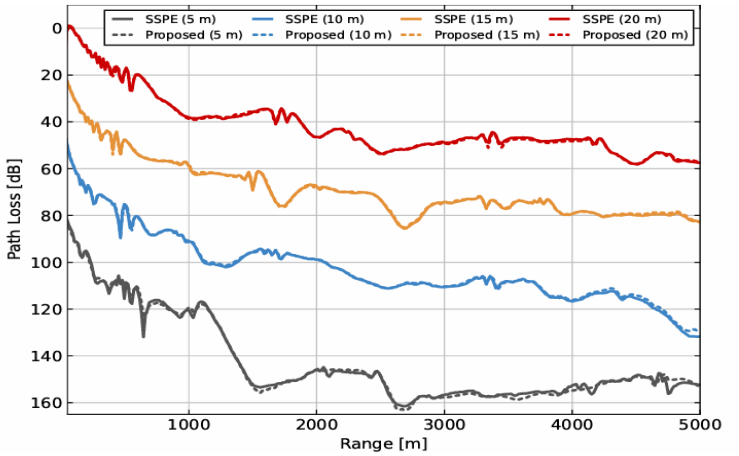
This section highlights the exceptional generalization capability of the proposed model when applied to previously unseen data. Specifically, during model evaluation, the prediction is considered interpolation if the test sample falls within the range of the training data, and extrapolation if it lies outside that range [35–39]. Although the concept of extrapolation is often neglected in many machine learning applications within electromagnetics, evaluating extrapolation generalizability is essential. It determines whether the framework can generate reliable results across a broad spectrum and assesses if the model truly understands the underlying electromagnetic relationships, rather than simply executing a regression task.

The results are illustrated in Figure 8. To evaluate the model's ability to generalize to specific parameters, we deliberately excluded data with particular parameter values from the training set, retrained the model, and then tested its performance on those previously unseen values. Since the terrain profiles were generated using random noise, all tests involving terrain shape represent extrapolation. For this, we selected three profiles with slope angles of $\theta = -0.3$, 0, and 0.3—referred to as downward, flat, and upward in Figure 8. For assessing generalization with respect to antenna height, we omitted data with heights of 5–7 m, 10 m, 15 m, and 18–20 m (as listed in Table 1), retrained the model, and then tested on heights of 5 m and 20 m (extrapolation), and 10 m and 15 m (interpolation). For antenna tilt angle, we excluded samples with tilt angles of 0–2°, 5°, 10°, and 13–15°, retrained the model, and evaluated extrapolation at 0° and 15°, and interpolation at 5° and 20°. For antenna beamwidth, data entries with beamwidths of 15–17°, 20°, 25°, and 28–30° were removed. The model was then tested on 15° and 30° for extrapolation, and 20° and 25° for interpolation. As shown in Figure 8, the model consistently delivers accurate predictions across various terrain types and antenna settings. Notably, it can extrapolate effectively to inputs up to 1.67 times beyond the range of the training data, underscoring its strong generalization capability.

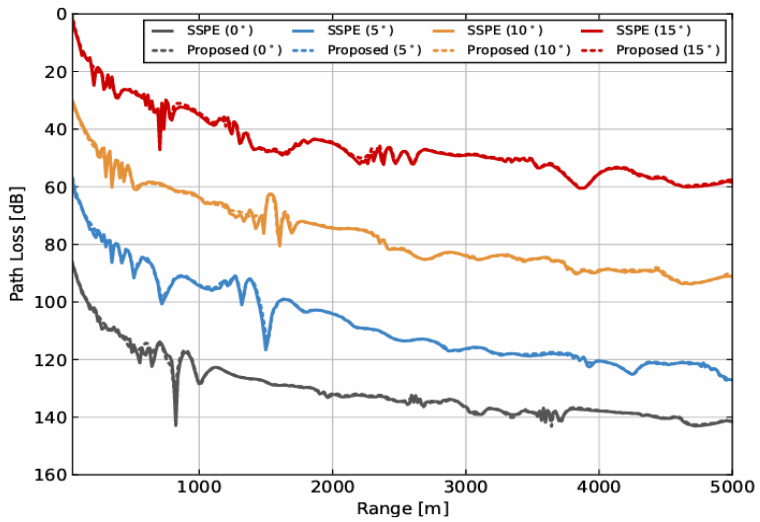


(**a**)

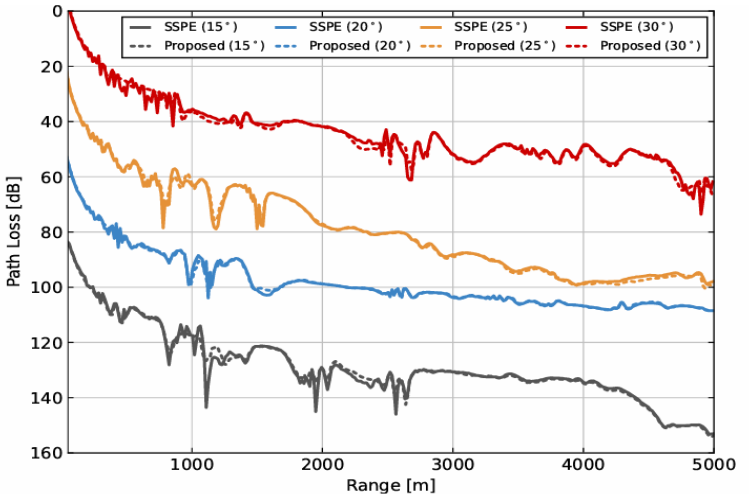
Figure 8. *Cont.*



(**b**)



(**c**)



(**d**)

Figure 8. (**a**) Path loss predictions over a randomly generated terrain, with the antenna positioned at a height of 10 m, a 3 dB beamwidth of 15°, and a tilt angle of 0° (terrain profile scalability). (**b**) Path loss predictions for varying antenna heights, while maintaining a 3 dB beamwidth of 15° and a tilt angle of 0° (antenna height scalability). (**c**) Path loss predictions with the antenna placed at a height of 15 m, using a 3 dB beamwidth of 25°, and varying tilt angles (antenna tilt angle scalability). (**d**) Path loss predictions with the antenna positioned at a height of 20 m, for different 3 dB beamwidths and a fixed tilt angle of 0° (antenna beamwidth scalability).

4. Use Cases in Complex Real-World Terrains

The proposed model has been validated using measurement data collected over two real-world irregular terrains in northern Denmark [34], as depicted in Figures 9–12. The selected terrain profiles—Hjorringvej and Jerslev—are shown in Figures 9 and 11, with lengths of 10 km and 5 km, respectively. These terrains were modeled as lossy dielectrics, using a relative permittivity of $\epsilon_r = 4.5$ and a loss tangent of $\tan \delta = 0.07$. The operating frequencies used in the simulations were 970 MHz for the Hjorringvej profile and 435 MHz for the Jerslev profile. Further technical details are available in [34].

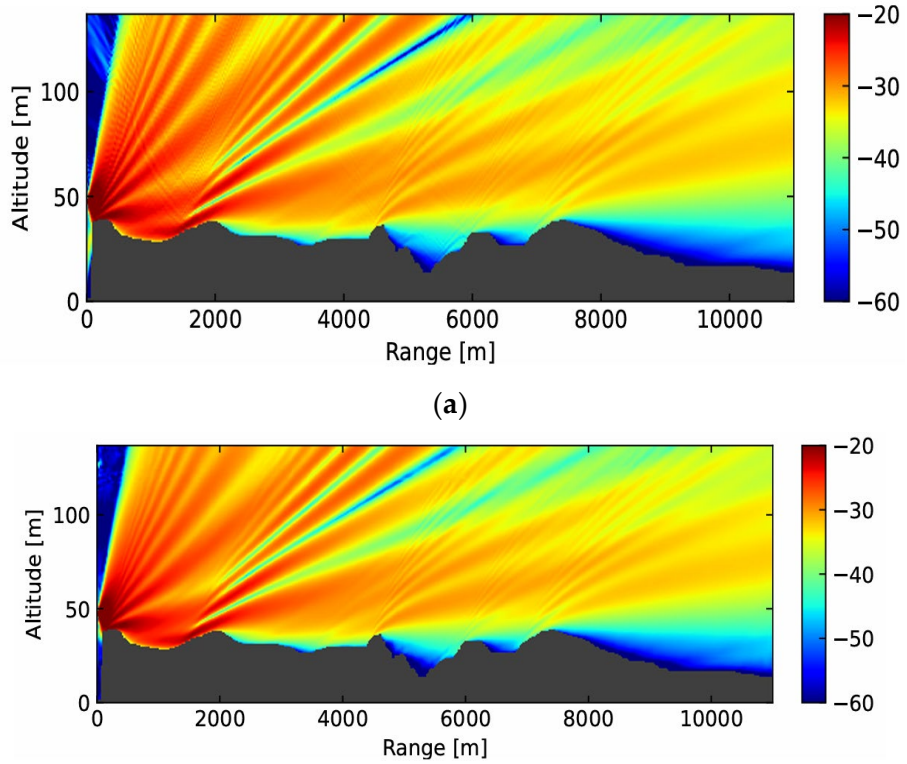


Figure 9. Field distribution maps for the Hjorringvej terrain: (**a**) using the SSPE method, and (**b**) using the proposed model.

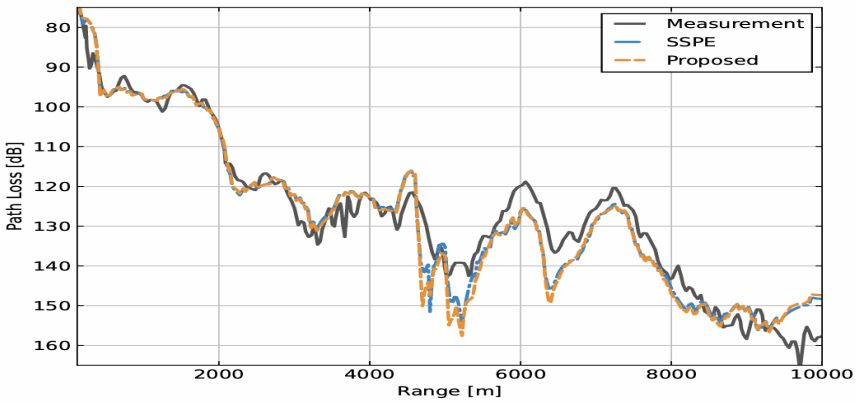


Figure 10. Signal attenuation across the Hjorringvej terrain.

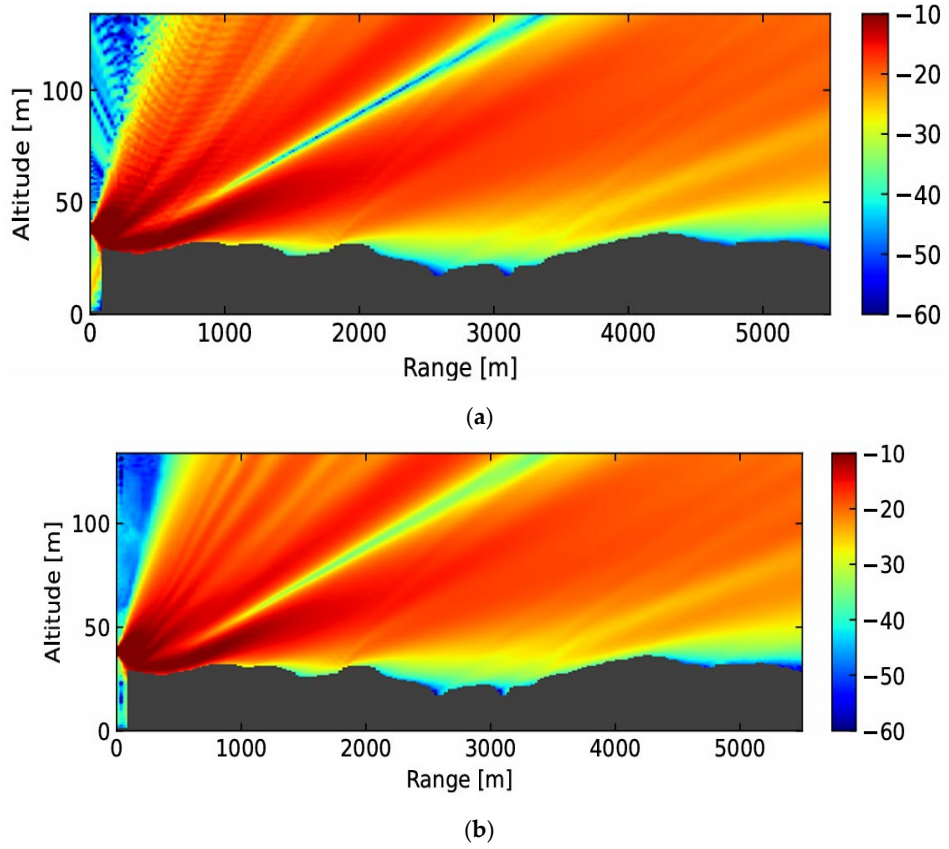


Figure 11. Electric field distribution maps over the Jerslev terrain: (**a**) using the SSPE method and (**b**) using the proposed approach.

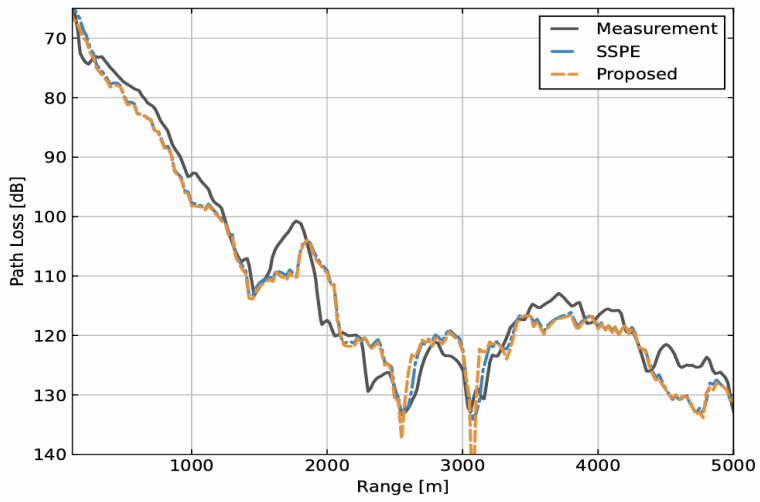


Figure 12. Signal attenuation along the Jerslev terrain profile.

Since these frequencies differ from those used during the initial model training, a new dataset was generated and the model was retrained. In this updated dataset, antenna parameters were kept constant, while terrain profiles were again generated using Perlin noise.

The path loss results predicted by the proposed model for both terrain profiles show strong agreement with the measurement data and with predictions from the traditional SSPE method. Notably, the proposed model completed the simulations in 99 s for Hjorringvej and 19 s for Jerslev, compared to 0.041 s and 0.037 s required by the SSPE approach. Despite the higher runtime, this demonstrates the model's effectiveness in accurately

simulating wave propagation over complex terrain while offering the flexibility of data-driven approaches.

In conclusion, the embedding strategy's actual advantage over more standard approaches is as follows. The proposed approach is designed to (i) capture richer structural and contextual information from the data, (ii) improve the representation of complex relationships among features, and (iii) enhance the model's predictive performance and robustness compared with standard embedding methods.

5. Conclusions, Limitations, and Future Directions

In this study, we present a scalable, physics-informed propagation modeling framework that maintains high accuracy across various terrain types and antenna setups. Our method significantly improves the efficiency of received signal strength prediction in complex landscapes. The core innovation lies in a novel parameter embedding approach that leverages prior knowledge from deterministic models, enhancing both accuracy and scalability. We also propose a spatial context encoding technique suited for large-scale modeling and develop a specialized network architecture optimized for terrain-related propagation challenges. The effectiveness of each component in our framework is validated through detailed ablation studies. Comparative analyses with numerical simulations confirm the model's appreciable scalability performance across different parameter settings. In addition, real-world validation using data from two irregular terrain environments further supports the model's reliability.

One key limitation is the model's dependency on the maximum terrain length defined during training. While padding can address shorter terrain profiles during testing, significantly longer terrains require the development of a new dataset and retraining. Moreover, the proposed model does not yet incorporate atmospheric or surface condition variability—an area identified for future exploration. Furthermore, extending the scalability across frequency bands and antenna types and improving scalability through multi-resolution and GIS-integrated modeling are areas to be explored. Further advancements may involve hybrid physics-AI fusion, online learning for real-time adaptation, and transfer learning across diverse terrains. Additionally, optimizing for edge deployment and embedding uncertainty quantification and interpretability features will be essential for robust, scalable, and explainable terrain-aware propagation modeling.

Author Contributions: Conceptualization, O.J.F. and M.O.O.; methodology, O.J.F.; software, E.E.; validation, O.J.F., M.O.O. and E.E.; formal analysis, O.J.F.; investigation, O.J.F.; resources, E.E.; writing—original draft preparation, O.J.F.; writing—review and editing, M.O.O.; supervision, O.J.F. and E.E.; funding acquisition, E.E. All authors have read and agreed to the published version of the manuscript.

Funding: The APC was funded by the University of South Africa.

Data Availability Statement: The data is available upon reasonable request.

Conflicts of Interest: The authors declare no conflicts of interest.

References

1. Da Costa, F.M.; Ramirez, L.A.R.; Dias, M.H.C. Analysis of ITU-R VHF/UHF propagation prediction methods performance on irregular terrains covered by forest. *IET Microw. Antennas Propag.* **2018**, *12*, 1450–1455. [CrossRef]
2. Sun, S.; MacCartney, G.R.; Rappaport, T.S. Investigation of prediction accuracy, sensitivity, and parameter stability of large-scale propagation path loss models for 5G wireless communications. *IEEE Trans. Veh. Technol.* **2016**, *65*, 2843–2860. [CrossRef]
3. Levy, M.F. *Parabolic Equation Methods for Electromagnetic Wave Propagation*; IET Electomagnetic Waves Series; The Institution of Engineering and Technology (IET): London, UK, 2000; ISBN 978-0-85296-764-5.
4. Apaydin, G.; Sevgi, L. *Radio Wave Propagation and Parabolic Equation Modeling*; Wiley-IEEE Press: Hoboken, NJ, USA, 2017; ISBN 978-1-119-43211-1.

5. Ozgun, O. Recursive Two-Way Parabolic Equation Approach for Modeling Terrain Effects in Tropospheric Propagation. *IEEE Trans. Antennas Propag.* **2009**, *57*, 2706–2714. [CrossRef]
6. Ozgun, O.; Apaydin, G.; Kuzuoglu, M.; Sevgi, L. PETOOL: MATLAB-Based One-Way and Two-Way Split-Step Parabolic Equation Tool for Radiowave Propagation over Variable Terrain. *Comput. Phys. Commun.* **2011**, *182*, 2638–2654. [CrossRef]
7. Wang, K.; Long, Y. Propagation Modeling over Irregular Terrain by the Improved Two-Way Parabolic Equation Method. *IEEE Trans. Antennas Propag.* **2012**, *60*, 4467–4471. [CrossRef]
8. Mylonakis, C.M.; Kantartzis, N.V.; Goudos, S.K.; Lazaridis, P.I.; Sarigiannidis, P.; Di Renzo, M.; Zaharis, Z.D. Multi-horizon direction of arrival forecasting with temporal fusion transformers: A time-series learning approach to target tracking. *IEEE Trans. Commun.* **2026**, *74*, 6687–6702. [CrossRef]
9. Seo, J.; Kang, C.; Seo, D.; Chung, H. Generalizing deep surrogate solvers for broadband electromagnetic field prediction at unseen wavelengths. *arXiv* **2024**, arXiv:2408.02971.
10. Famoriji, O.J.; Shongwe, T. Simple and effective electromagnetic wave propagation loss model in GSM band for smart campus applications. *SSRG Int. J. Electr. Electron. Eng.* **2024**, *11*, 306–311. [CrossRef]
11. Famoriji, O.J.; Shongwe, T. Deep Learning Assisted Radiowave Propagation Loss Prediction in the Tropics. In Proceedings of the 5th International Conference on Electrical, Computer and Energy Technologies, Paris, France, 3–6 July 2025. [CrossRef]
12. Ma, Z.; Xu, K.; Song, R.; Wang, C.-F.; Chen, X. Learning-based fast electromagnetic scattering solver through generative adversarial network. *IEEE Trans. Antennas Propag.* **2020**, *69*, 2194–2208. [CrossRef]
13. Shan, T.; Zeng, J.; Song, X.; Guo, R.; Li, M.; Yang, F.; Xu, S. Physics informed supervised residual learning for electromagnetic modeling. *IEEE Trans. Antennas Propag.* **2023**, *71*, 3393–3407. [CrossRef]
14. Liu, S.; Onishi, T.; Taki, M.; Watanabe, S. A generalizable indoor propagation model based on graph neural networks. *IEEE Trans. Antennas Propag.* **2023**, *71*, 6098–6110. [CrossRef]
15. Seretis, A.; Sarris, C.D. Toward physics-based generalizable convolutional neural network models for indoor propagation. *IEEE Trans. Antennas Propag.* **2022**, *70*, 4112–4126. [CrossRef]
16. Brennan, C.; Cullen, P.J.; Rossi, L. An MFIE-based tabulated interaction method for UHF terrain propagation problems. *IEEE Trans. Antennas Propag.* **2000**, *48*, 1003–1005. [CrossRef]
17. Famoriji, O.J.; Shongwe, T. Icosahedral CNN for DoA Estimation of EM Wave Sources Arriving Spherical Antenna Array Incorporating the Impact of Mutual. Coupling. In Proceedings of the 4th International Conference on Electrical, Computer and Energy Technologies, Sydney, Australia, 25–27 July 2024. [CrossRef]
18. Bakirtzis, S.; Chen, J.; Qiu, K.; Zhang, J.; Wassell, I. EM deepray: An expedient, generalizable, and realistic data-driven indoor propagation model. *IEEE Trans. Antennas Propag.* **2022**, *70*, 4140–4154. [CrossRef]
19. Seretis, A.; Jevremovic, V.; Jemmali, A.; Sarris, C.D. Generalizable machine-learning based modeling of radiowave propagation in stadiums. *IEEE Open J. Antennas Propag.* **2023**, *4*, 1116–1128. [CrossRef]
20. Famoriji, O.J.; Shongwe, T. Physics-Informed Analytical Framework for Design and Optimization of a Dual-Radius Spherical Antenna Array under Mutual Coupling. *SSRG Int. J. Electr. Electron. Eng.* **2025**, *12*, 125–135. [CrossRef]
21. Ratnam, V.V.; Chen, H.; Pawar, S.; Zhang, B.; Zhang, C.J.; Kim, Y.-J.; Lee, S.; Cho, M.; Yoon, S.-R. Fadenet: Deep learning-based mm wave large-scale channel fading prediction and its applications. *IEEE Access* **2020**, *9*, 3278–3290.
22. Mao, Y.; Zhan, Q.; Zhang, R.; Wang, D.; Huang, W.-F.; Liu, Q.H. Fast simulation of electromagnetic fields in doubly periodic structures with a deep fully convolutional network. *IEEE Trans. Antennas Propag.* **2020**, *69*, 2921–2928. [CrossRef]
23. Famoriji, O.J.; Shongwe, T. Deep Learning Approach to Source Localization of Electromagnetic Waves in the Presence of Various Sources and Noise. *Symmetry* **2023**, *15*, 1534. [CrossRef]
24. Yao, H.M.; Jiang, L.; Ng, M. Implementing the fast full-wave electromagnetic forward solver using the deep convolutional encoder decoder architecture. *IEEE Trans. Antennas Propag.* **2022**, *71*, 1152–1157. [CrossRef]
25. Bernardi, P.; Caratelli, D.; Cicchetti, R.; Schena, V.; Testa, A. A numerical scheme for the solution of the vector parabolic equation governing the radio wave propagation in straight and curved rectangular tunnels. *IEEE Trans. Antennas Propag.* **2009**, *57*, 3249–3257. [CrossRef]
26. Chen, L.-C.; Zhu, Y.; Papandreou, G.; Schroff, F.; Adam, H. Encoder decoder with atrous separable convolution for semantic image segmentation. In Proceedings of the European Conference on Computer Vision (ECCV), Munich, Germany, 8–14 September 2018; pp. 801–818.
27. Huang, H.; Lin, L.; Tong, R.; Hu, H.; Zhang, Q.; Iwamoto, Y.; Han, X.; Chen, Y.-W.; Wu, J. Unet 3+: A full-scale connected unet for medical image segmentation. In Proceedings of the IEEE International Conference on Acoustics, Speech and Signal Processing (ICASSP), Virtual, 4–8 May 2020; pp. 1055–1059.
28. Tang, Z.; Peng, X.; Li, K.; Metaxas, D.N. Towards efficient u-nets: A coupled and quantized approach. *IEEE Trans. Pattern Anal. Mach. Intell.* **2019**, *42*, 2038–2050. [CrossRef] [PubMed]
29. Qin, X.; Zhang, Z.; Huang, C.; Dehghan, M.; Zaiane, O.R.; Jagersand, M. U2-net: Going deeper with nested u-structure for salient object detection. *Pattern Recognit.* **2020**, *106*, 107404. [CrossRef]

30. Wu, X.; Hong, D.; Chanussot, J. Uiu-net: U-net in u-net for infrared small object detection. *IEEE Trans. Image Process.* **2022**, *32*, 364–376. [PubMed]
31. Perlin, K. An image synthesizer. *ACM Siggraph Comput. Graph.* **1985**, *19*, 287–296. [CrossRef]
32. Burger, W.; Burge, M.J. *Principles of Digital Image Processing: Advanced Methods*; Springer Science & Business Media: Berlin/Heidelberg, Germany, 2013.
33. Laine, A.F.; Zong, X. Multiscale suboctave wavelet transform for denoising and enhancement. In *Wavelet Applications in Signal and Image Processing IV*; SPIE: Bellingham, WA, USA, 1996; Volume 2825, pp. 238–249.
34. Hviid, J.T.; Andersen, J.B.; Toftgard, J.; Bojer, J. Terrain-based propagation model for rural area-an integral equation approach. *IEEE Trans. Antennas Propag.* **1995**, *43*, 41–46. [CrossRef]
35. Famoriji, O.J.; Shongwe, T. An Effective Antenna Array Diagnosis Method via Multivalued Neural Network Inverse Modeling Approach. *Adv. Electromagn.* **2021**, *10*, 58–70. [CrossRef]
36. Chen, L.-C.; Papandreou, G.; Kokkinos, I.; Murphy, K.; Yuille, A.L. Deeplab: Semantic image segmentation with deep convolutional nets, atrous convolution, and fully connected crfs. *IEEE Trans. Pattern Anal. Mach. Intell.* **2017**, *40*, 834–848. [CrossRef] [PubMed]
37. Zhu, Q.; Du, B.; Turkbey, B.; Choyke, P.L.; Yan, P. Deeply-supervised CNN for prostate segmentation. In Proceedings of the International Joint Conference on Neural Networks, Anchorage, AK, USA, 14–19 May 2017; pp. 178–184.
38. Elmahdy, M.S.; Beljaards, L.; Yousefi, S.; Sokooti, H.; Verbeek, F.; Van Der Heide, U.A.; Staring, M. Joint registration and segmentation via multi-task learning for adaptive radiotherapy of prostate cancer. *IEEE Access* **2021**, *9*, 95551–95568. [CrossRef]
39. Liu, Y.; Yang, G.; Mirak, S.A.; Hosseiny, M.; Azadikhah, A.; Zhong, X.; Reiter, R.E.; Lee, Y.; Raman, S.S.; Sung, K. Automatic prostate zonal segmentation using fully convolutional network with feature pyramid attention. *IEEE Access* **2019**, *7*, 163626–163632. [CrossRef]

Disclaimer/Publisher's Note: The statements, opinions and data contained in all publications are solely those of the individual author(s) and contributor(s) and not of MDPI and/or the editor(s). MDPI and/or the editor(s) disclaim responsibility for any injury to people or property resulting from any ideas, methods, instructions or products referred to in the content.